

Transition from Flat-Band Localization to Anderson Localization in a One-Dimensional Tasaki Lattice

Chao Zeng,^{1,2,3} Yue-Ran Shi^{4,5}, Yi-Yi Mao^{1,2}, Fei-Fei Wu^{1,2}, Yan-Jun Xie^{1,2}, Tao Yuan,^{1,2} Wei Zhang,^{4,5,*}
Han-Ning Dai^{1,2,3,†}, Yu-Ao Chen,^{1,2,3,‡} and Jian-Wei Pan^{1,2,3,§}


¹Hefei National Research Center for Physical Sciences at the Microscale and School of Physical Sciences,
University of Science and Technology of China, Hefei 230026, China

²Shanghai Research Center for Quantum Sciences and CAS Center for Excellence in Quantum Information and Quantum Physics,
University of Science and Technology of China, Shanghai 201315, China

³Hefei National Laboratory, University of Science and Technology of China, Hefei 230088, China

⁴Department of Physics and Beijing Key Laboratory of Opto-electronic Functional Materials and Micro-nano Devices,
Renmin University of China, Beijing 100872, China

⁵Key Laboratory of Quantum State Construction and Manipulation (Ministry of Education),
Renmin University of China, Beijing 100872, China

 (Received 27 July 2023; revised 3 November 2023; accepted 4 December 2023; published 5 February 2024)

We report an extensive experimental investigation on the transition from flat-band localization (FBL) to Anderson localization (AL) in a one-dimensional synthetic lattice in the momentum dimension. By driving multiple Bragg processes between designated momentum states, an effective one-dimensional Tasaki lattice is implemented with highly tunable parameters, including nearest-neighbor and next-nearest-neighbor coupling coefficients and onsite energy potentials. With that, a flat-band localization phase is realized and demonstrated via the evolution dynamics of the particle population over different momentum states. The localization effect is undermined when a moderate disorder is introduced to the onsite potential and restored under a strong disorder. We find clear signatures of the FBL-AL transition in the density profile evolution, the inverse participation ratio, and the von Neumann entropy, where good agreement is obtained with theoretical predictions.

DOI: [10.1103/PhysRevLett.132.063401](https://doi.org/10.1103/PhysRevLett.132.063401)

Introduction.—The connection between disorder and localization in periodic lattices is a fundamental problem in many fields, such as condensed matter physics [1] and statistic physics [2–4]. Intuitively, the presence of disorder breaks translational symmetry and compromises the coherence of particle hopping. As a result, a sufficiently strong disorder would completely prohibit particle transport in arbitrary dimensions and lead to a localized phase referred to as Anderson localization (AL) [5]. Meanwhile, localization can also occur in a disorder-free system, where perfect destructive interference of particle hopping is induced by careful design of the lattice configuration to create a flat band with localized single-particle eigenstates [6,7]. This mechanism leads to a phenomenon called flat-band localization (FBL) or compact localization. Both AL and FBL can sustain a certain degree of interaction to enter a many-body localization state [8–13], which features nonergodic behaviors and breaks the eigenstate thermalization hypothesis [14,15]. However, theoretical analysis suggests that the many-body localization states that emerged from FBL and AL are distinct phases with different physical properties [16–18].

A system with FBL can be turned into an AL phase by introducing sufficiently strong disorder. In one and two

dimensions, an FBL-AL phase transition is predicted in noninteracting Fermi systems if the flat band is fully gapped from neighboring dispersive bands, with a critical disorder strength on the order of the energy gap [7,19]. On the other hand, a metallic phase may even exist in higher dimensions between the FBL and AL phases, resulting in a disorder-induced insulator-metal transition known as the inverse Anderson localization transition [20–22]. These theoretical investigations suggest a rather counterintuitive phenomenon that disorder can be detrimental to localization.

From an experimental perspective, flat-band systems have been realized in various systems, including metamaterials, cavity polaritons [23,24], photonic waveguides [25–28], and ultracold atoms in optical lattices [29–32]. However, the attempt to observe the FBL-AL transition requires precise control of the lattice potential at a single-site level and the ability to measure time-dependent transport behavior, which is absent in most solid-state systems. Artificial lattices, such as photonic waveguides and synthetic atomic lattices [32,33], allow for simulating flat-band systems in a more controllable manner. For example, a scheme has been recently proposed for photonic crystals, where the quantum behavior of wave functions can be simulated by classical light waves owing to the similarity

between the electromagnetic wave equation and the Schrödinger equation [21].

Here, we report an extensive experimental investigation on the FBL-AL transition with a Bose-Einstein condensate (BEC) of ^{87}Rb atoms in a one-dimensional (1D) momentum lattice, as shown in Fig. 1(a). Using different momentum states to denote lattice sites, we tune the two- and four-photon Bragg scattering lasers [34–38] to realize precise control of the hopping rates between individual sites and the position-dependent onsite potential. The time-dependent probability distribution with a single-site resolution can be measured via the time-of-flight technique. We first realize a 1D Tasaki lattice [39] with 12 unit cells (25 lattice sites), and observe a nondiffusive behavior when the system is initialized at an eigenstate of the flat band. Then we introduce an effective disorder potential by changing the detuning of Bragg processes to witness the FBL-AL transition from the time evolution of particle distribution. The transition is characterized by the “efficiency” parameter, the inverse participation ratio, and the von Neumann entropy, all showing good agreement with numerical simulations. Our work not only deepens the understanding of the relationship between disorder and localization, which has remained one of the central topics in the study of metal-insulator transition for decades, but also shows the ability of the momentum lattice as a versatile platform to study transport properties in artificial geometries.

Tasaki lattice and experimental realization.—The 1D Tasaki lattice, also called the sawtooth lattice, comprises two types of sites, labeled A and B , as illustrated in Fig. 1(b). Particles can hop between A and B sites if they are nearest neighbors and from a B site to the two nearest B sites. For a system with L unit cells, each containing an A site and a B site, there are in total $2L - 1$ tunneling terms between A and B with coefficients u , and $L - 1$ terms between B and B with hopping rate v . The Hamiltonian reads

$$H_{\text{Tasaki}} = \sum_i \left(u \hat{c}_{i,A}^\dagger c_{i,B} + u \hat{c}_{i,A}^\dagger \hat{c}_{i+1,B} + \text{H.c.} \right) + \sum_i \left(v \hat{c}_{i,B}^\dagger \hat{c}_{i+1,B} + \text{H.c.} \right) + \sum_{i,s} W_{i,s} \hat{c}_{i,s}^\dagger \hat{c}_{i,s}, \quad (1)$$

where $\hat{c}_{i,s}^\dagger$ and $\hat{c}_{i,s}$ are the creation and annihilation operators for particles on the $s = A, B$ site of the i th unit cell, $W_{i,s}$ is the onsite energy offset describing a disorder potential, and H.c. stands for Hermitian conjugate. In the absence of disorder $W_{i,s} = 0$, the single particle dispersion presents two bands

$$E_{\pm} = |v| \cos k \pm \sqrt{|v|^2 \cos^2 k + 2|u|^2(1 + \cos k)}. \quad (2)$$

When the tunneling coefficients satisfy $r \equiv |u|/|v| = \sqrt{2}$, the lower band is completely flat with $E_- = -2|v|$, as

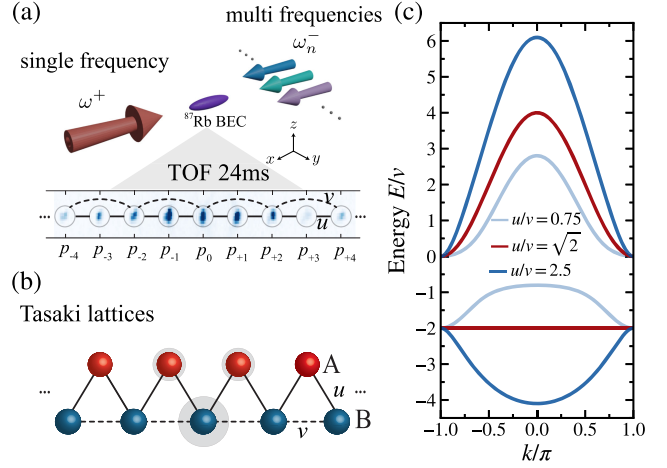


FIG. 1. Realization of 1D Tasaki lattice with onsite disorder in momentum lattice. (a) A 1D momentum lattice realized using Bragg processes (top) and visualized via time-of-flight imaging (bottom). (b) A 1D Tasaki lattice is composed of two sublattices with hopping integrals u and v . (c) The energy bands of 1D Tasaki lattice with increasing ratios $r \equiv |u|/|v| = 0.75, \sqrt{2}, 2.5$ (from the middle to both sides). A fully gapped flat band is realized with $r = \sqrt{2} \approx 1.4$ (red lines).

shown in Fig. 1(c). The single particle eigenstates of the flat band are $|\phi_i\rangle = [-\frac{1}{2}\hat{c}_{i-1,A}^\dagger + (\sqrt{2}/2)\hat{c}_{i,B}^\dagger - \frac{1}{2}\hat{c}_{i,A}^\dagger]|\text{vac}\rangle$ with $|\text{vac}\rangle$ the vacuum state, which are completely localized due to the destructive interference of hopping. The existence of disorder would inevitably spoil this destructive interference by coupling the FBL state to other dispersive Bloch waves. When strong enough disorder $W_{i,s}$ is present, the single-particle states become the localized states associated with the disorder potential, and the system enters the AL phase.

To characterize the FBL-AL transition, a localization length ξ can be defined from the asymptotic exponential decay of a single-particle wave function [40] $\psi_j^{i,(A,B)} \propto \exp(-j/\xi)$, which presents different scaling behaviors for the FBL and AL phases [7,19]. In Fig. 2, we show for example the localization length of the eigenstate with $E = -2|v|$ in units of lattice constant, where two different power-law behaviors $\xi(W) \sim W^\gamma$ can be clearly observed. Here, W represents the dimensionless disorder strength in units of $|v|$ with $W_{i,s} = m_{i,s}W|v|$, and $m_{i,s}$ is a random number uniformly distributed within $[-1, 1]$. In the weak disorder limit, ξ is nearly a constant with $\gamma = 0$, which is determined by the nature of the compact localized state. For strong disorder with $W \gtrsim 2$, the exponent becomes $\gamma \approx -0.5$ characterizing an AL phase. The FBL-AL transition occurs when the disorder strength approaches the band gap [41,42].

In our experiment, we implement the Hamiltonian Eq. (1) in an optically trapped ^{87}Rb BEC, which is driven by counter-propagating lasers with wavelength $\lambda = 1064$ nm

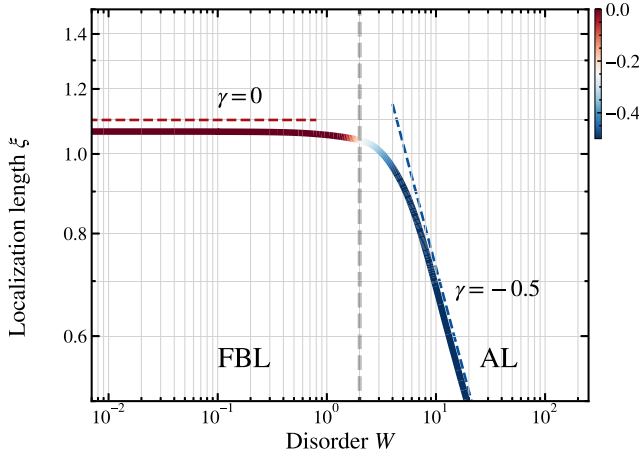


FIG. 2. Localization length $\xi(W)$ (in units of lattice constant) for the eigenstate of $E = -2|v|$. The result is for a system with size $N = 1001$ and an average of 100 disorder configurations $|W_{i,s}| < W$. The power-law exponent γ (false color) changes from 0 for FBL to -0.5 for AL.

and wave number $k = 2\pi/\lambda$. The laser along one direction has a single frequency component, while the opposite beam is engineered to contain multiple discrete frequency components, matching the two-photon and four-photon Bragg resonance conditions for states with linear momenta $p_n = 2n\hbar k$. These momentum states form a 1D synthetic lattice, where particles can transfer between different states $|n\rangle$ with momentum p_n according to the time-dependent Hamiltonian

$$H(t) = \sum_n \left[\left(K(t) \hat{c}_{n+1}^\dagger \hat{c}_n + \text{H.c.} \right) + E_n \hat{c}_n^\dagger \hat{c}_n \right]. \quad (3)$$

The tunneling coefficient reads

$$K(t) = \hbar \sum_j (K_{ju} + K_{jv_1} + K_{jv_2}), \quad K_{js} = \Omega_{js} e^{-i\omega_{js}t}, \quad (4)$$

where Ω_{js} is the Rabi frequency with the j th frequency component, and ω_{js} denotes the frequency difference between the two lasers driving the $|j\rangle \leftrightarrow |j+1\rangle$ transition. The term with $s = u$ represents the two-photon Bragg process inducing nearest neighbor hopping, while the terms with $s = v_1$ and v_2 are the components of the four-photon transitions between next-nearest-neighbor sites. Here, $E_n = 4n^2 E_r$ is the energy of the n th momentum state. More details of the derivation of the effective Hamiltonian can be found in the Ref. [41].

Flat-band localization.—To observe the phenomenon of FBL, we first implement a Tasaki lattice in momentum space and optimize the ratio parameter r to realize a flat band. Here, we individually address and tune the transition between an arbitrary pair of momentum states by Bragg lasers. With such controllability, we use a total of 24 appropriate frequencies to generate tunneling between

states $|n\rangle$ with momentum $p_n = 2n\hbar k$ and its nearest neighbors $|n \pm 1\rangle$ for $n = 0, \pm 1, \dots, \pm 11$, and an additional 18 beams to create hopping between $|m\rangle$ and $|m \pm 2\rangle$ for $m = 0, \pm 2, \dots, \pm 10$. In that configuration, the states with odd momentum index n are classified as the A sites, while the ones with even n act as the B sites. We fix the hopping rate between the B sites at $|v| \approx 2\pi\hbar \times 0.2$ kHz and tune the tunneling strength $|u|$ and its relative phase.

To demonstrate the localization effect, we study the time evolution of an initial state $|\phi_i\rangle$. We start from a BEC in the zero momentum state $|n = 0\rangle$ with total number N , and turn on the coupling to the $|-1\rangle$ state with tunneling strength $2\pi\hbar \times 0.5$ kHz and phase -0.4π , and to the $|+1\rangle$ state with the same strength but an opposite phase 0.4π for a duration about $\sqrt{2}/8$ ms [41]. This process produces with very high fidelity the state $|\phi_0\rangle = (-\frac{1}{2}| -1\rangle + (\frac{\sqrt{2}}{2})|0\rangle - \frac{1}{2}|+1\rangle)$, which is an eigenstate of the lower flat band of the Tasaki lattice for $r = \sqrt{2}$. In the thermodynamic limit, such a state would be completely localized at its original spots without any diffusion because tunneling to other sites is coherently destructive. In Figs. 3(a) and 3(b), we show the experimental data and numerical simulations of the normalized occupation

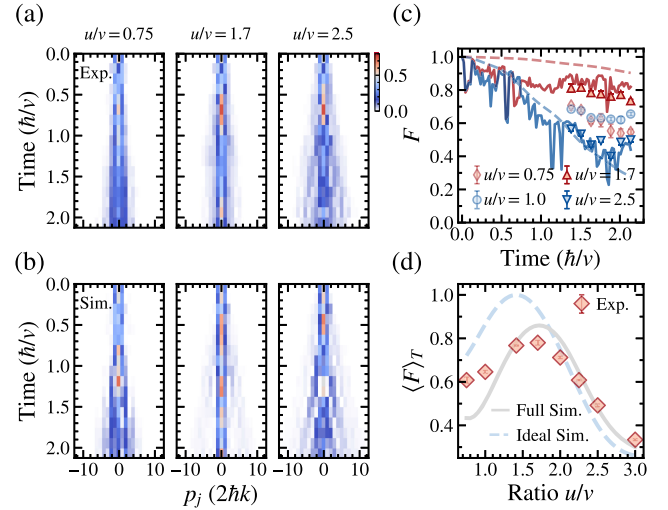


FIG. 3. (a) The particle populations (false color) of different sites upon time evolution are measured for cases of $r = 0.75, 1.7$, and 2.5 . (b) The same results obtained from numerical simulation of the time-dependent Hamiltonian Eq. (3). Both panels are taken with $|v| \approx 2\pi\hbar \times 0.2$ kHz in a Tasaki lattice of 25 sites. (c) Experimental time evolution of the efficiency F for $r = 0.75, 1.0, 1.7$, and 2.5 (circles with error bars). The red and blue solid (dashed) lines represent the numerical simulation results of the time-dependent Hamiltonian (effective Tasaki lattice) for $r = 1.7$ and 2.5 , respectively. (d) Time averaged efficiency $\langle F \rangle_T$ as a function of r . Experimental data (red diamonds with error bars smaller than the size of symbols) are averaged in time over the range $1.375\hbar/|v|$ to $2.125\hbar/|v|$ in a step of $0.125\hbar/|v|$. The results of numerical simulation based upon the time-dependent Hamiltonian (solid) and effective Tasaki lattice (dashed) are depicted for comparison.

of different momentum states $P_n(t) = \langle n|n\rangle/N$ over time starting from $|\phi_0\rangle$. The results show an apparent localization effect for $r \approx 1.7$, where the significant population is kept within the center three momentum states during the evolution. This value is slightly different from the theoretical parameter $r = \sqrt{2}$, mainly due to the presence of interatomic interaction as well as nonidealities [41,42].

To quantify the localization effect, we define the ‘‘efficiency’’ F as described in Ref. [43], in terms of the normalized number of atoms P_n^m of a given state m detected at lattice site n

$$F_m = \left(\sum_n \sqrt{P_n^{m,\text{Tasaki}} P_n^{m,\text{expt}}} \right)^2, \quad (5)$$

where the results for a Tasaki lattice $P_n^{m,\text{Tasaki}}$ and for the experimental system $P_n^{m,\text{expt}}$ are both used. For an infinitely long 1D Tasaki lattice with a perfect flat band, F should remain unity, reflecting complete localization. However, a numerical simulation of the time-dependent Hamiltonian Eq. (3) of a finite size prepared in our experiment suggests that F becomes lower than 1 and oscillates over time for short time as shown in Fig. 3(c), and saturates to an asymptotic trend for a sufficiently long time. That is, the initial state undergoes inevitable diffusion for all realizations. For a typical choice of evolving time $t = 2.125\hbar/|v|$ (~ 1.7 ms), which is long enough so that the oscillation of particle distributions is smeared out and the time dependence of F shows a smooth trend, the time averaged efficiency $\langle F \rangle_T$ reaches its maximum of ~ 0.85 at $r \approx 1.7$ [gray line in Fig. 3(d)]. The experimental measurements (red diamonds with error bars) reveal the expected behavior by changing r and show good agreement with the numerical simulations, except for the region of small ratio where the nonlinear effect of interatomic interaction and global trapping potential can be significant.

Transition to Anderson localization.—Next, we introduce a site-dependent potential $W_{i,s}$ to investigate the diffusion of particles from the disorder-free limit of FBL to the AL regime with strong disorder. For this purpose, we tune the frequency and power of the Bragg lasers to produce a detuning to the transitions between different momentum sites. By choosing a proper set of laser parameters, such detuning can be described as the onsite energy offset $W_{i,s}$ as given in Eq. (1). To analyze the disorder effect, we generate an ensemble of different configurations $\{W_{i,s}\} = \{m_{i,s}W\}$, where $m_{i,s} \in [-1, 1]$. By fixing r at 1.7, we increase W from zero and measure the efficiency F at $t = 2.125\hbar/|v|$ (~ 1.7 ms).

We display in Fig. 4(a) a false-colored plot of $\langle F \rangle$ obtained by simulation with varying r and W , where the FBL phase (i) is separated from the AL phase (iii) by a transition region (ii). In Fig. 4(b), we show the disorder averaged efficiency $\langle F \rangle$ for 16 different choices of W ranging from 0.01 to 200. For each data point, an average

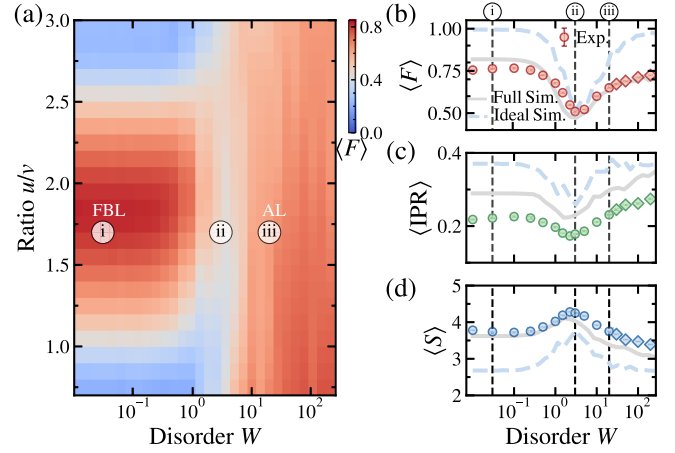


FIG. 4. (a) False-colored plot of the disorder averaged efficiency $\langle F \rangle$ obtained from numerical simulation of the time-dependent Hamiltonian Eq. (3) for $t = 2.125\hbar/|v|$ (~ 1.7 ms). By varying the disorder strength W and the hopping ratio r , two localized regions (red) labeled by (i) and (iii) can be identified and are separated by a crossover region labeled by (ii). (b) When increasing W with a fixed $r \approx 1.7$, the measured results of $\langle F \rangle$ (red circle) agree well with numerical simulation (gray line), and signature the transition from FBL (i) to AL (iii). All data are averaged over 50 independent disorder configurations after evolving for $t = 2.125\hbar/|v|$. (c) The IPR \mathcal{I} and (d) the von Neumann entropy \mathcal{S} of a given initial state as a function of W . Symbols represent experimental data averaged over 50 independent disorder configurations after evolving for $t = 2.125\hbar/|v|$. The results of numerical simulation based upon the time-dependent Hamiltonian (solid) and effective Tasaki lattice (dashed) are depicted for comparison. The error bars of experimental results are all smaller than the size of the symbol in panels (b)–(d).

over 50 sampling configurations is taken, and the convergence of both the average and variance is confirmed by numerical simulation and experimental data. In this plot, three different regions can be identified. The region labeled by (i) features a large $\langle F \rangle$, which nearly remains constant at approximately 0.75 for $W \lesssim 0.5$. This observation indicates that the mechanism of FBL, i.e., destructive interference of hopping, still dominates and that the initial state is only slightly modified upon evolution in the presence of weak disorder. When W is increased above 0.5, $\langle F \rangle$ starts to drop and reaches a minimum of ~ 0.51 at $W \approx 3$, beyond which it is quickly restored. In this region [labeled by (ii)], disorder compromises the destructive interference such that the final state upon evolution is significantly modified from its origin. However, a theoretical analysis of level statistics confirms that the system is still in a localized phase with a Poisson distribution [41]. As W is further increased over ~ 10 , the disorder is strong enough to dominate the background lattice structure. In this region denoted by (iii), the system enters the AL phase, where particle transport is prohibited. For even larger $W > 20$, the disorder potential becomes comparable or even exceeds the recoil energy and

the frequency difference between different Bragg transitions. In this case, multiple transition processes must be considered and the effective momentum lattice model of Eq. (1) is no longer valid. Nonetheless, the system remains in the AL phase as witnessed in Figs. 4(b)–4(d), where the experimental data are presented by a different type of symbol.

To further characterize the FBL-AL transition, we analyze two measures of localization, including the inverse participation ratio (IPR) \mathcal{I} and the von Neumann entropy \mathcal{S} , defined as [8]

$$\mathcal{I} = \sum_n P_n^2, \quad (6)$$

$$\mathcal{S} = \sum_n [-P_n \log_2(P_n) - (1 - P_n) \log_2(1 - P_n)], \quad (7)$$

where the summation runs over all lattice sites. For a perfect flat band, the IPR of a given single-particle eigenstate $|\phi_0\rangle$ takes the maximal value of $\mathcal{I} = 3/8$ and does not change over time. In the presence of disorder, the disorder average of IPR $\langle \mathcal{I} \rangle$ becomes time-dependent and is reduced from this theoretical limit in both numerical simulation (gray solid line) and experimental measurement (circles), as shown in Fig. 4(c). One can clearly identify two plateaus of large IPR in the weak and strong disorder regions, corresponding to the FBL and AL phases, respectively. A transition region lies between the two localized phases, where the IPR presents a dip to as low as $\mathcal{I} \sim 0.15$. Similar behavior is observed in the results of von Neumann entropy for a given single-particle state, as shown in Fig. 4(d). A theoretical calculation suggests that the FBL-AL transition is more evident in the averaged $\tilde{\mathcal{I}}$ and $\tilde{\mathcal{S}}$ over the entire single-particle spectrum [8,17,41].

Summary.—We implement a one-dimensional Tasaki lattice in a momentum lattice of ultracold ^{87}Rb atoms. The experimental platform provides the ability to precisely control the strength and phase of tunneling between sites, as well as the onsite energy of individual sites. With that, we obtain a flat band phase and observe the localization effect of the initial state via time-of-flight imaging. We then introduce an onsite disorder potential and witness a transition from the FBL phase to the AL phase, which are both insulating states but induced by different mechanisms. The FBL-AL transition is further identified by the inverse participation ratio and the von Neumann entropy. The method can be naturally applied to construct other one-dimensional models with a composite basis, such as the diamond chain model, the zigzag model, and the Aharonov-Bohm caging model, where exotic topological [44,45] and transport properties [22] may be present.

This work is supported by the National Natural Science Foundation of China (Grants No. 12074367,

No. 12074428, and No. 92265208), Anhui Initiative in Quantum Information Technologies, the National Key Research and Development Program of China (Grants No. 2020YFA0309804 and No. 2018YFA0306501), Shanghai Municipal Science and Technology Major Project (Grant No. 2019SHZDZX01), Innovation Program for Quantum Science and Technology (Grant No. 2021ZD0302002), the Strategic Priority Research Program of Chinese Academy of Sciences (Grant No. XDB35020200), and the New Cornerstone Science Foundation.

C. Z. and Y.-R. S. contributed equally to this work.

*wzhangl@ruc.edu.cn

†daihan@ustc.edu.cn

‡yuaochen@ustc.edu.cn

§pan@ustc.edu.cn

- [1] A. Lagendijk, B. van Tiggelen, and D. S. Wiersma, *Phys. Today* **62**, No. 8, 24 (2009).
- [2] L. F. Santos and M. Rigol, *Phys. Rev. E* **81**, 036206 (2010).
- [3] E. Fratini and S. Pilati, *Phys. Rev. A* **92**, 063621 (2015).
- [4] T. Takaishi, K. Sakakibara, I. Ichinose, and T. Matsui, *Phys. Rev. B* **98**, 184204 (2018).
- [5] P. W. Anderson, *Phys. Rev.* **109**, 1492 (1958).
- [6] S. Flach, D. Leykam, J. D. Bodyfelt, P. Matthies, and A. S. Desyatnikov, *Europhys. Lett.* **105**, 30001 (2014).
- [7] D. Leykam, J. D. Bodyfelt, A. S. Desyatnikov, and S. Flach, *Eur. Phys. J. B* **90**, 1 (2017).
- [8] N. Roy, A. Ramachandran, and A. Sharma, *Phys. Rev. Res.* **2**, 043395 (2020).
- [9] T. Orito, Y. Kuno, and I. Ichinose, *Phys. Rev. B* **104**, 094202 (2021).
- [10] C. D’Errico, E. Lucioni, L. Tanzi, L. Gori, G. Roux, I. P. McCulloch, T. Giamarchi, M. Inguscio, and G. Modugno, *Phys. Rev. Lett.* **113**, 095301 (2014).
- [11] H. Yao, T. Giamarchi, and L. Sanchez-Palencia, *Phys. Rev. Lett.* **125**, 060401 (2020).
- [12] R. Gautier, H. Yao, and L. Sanchez-Palencia, *Phys. Rev. Lett.* **126**, 110401 (2021).
- [13] J.-C. Yu, S. Bhave, L. Reeve, B. Song, and U. Schneider, *arXiv:2303.00737*.
- [14] V. Oganessian and D. A. Huse, *Phys. Rev. B* **75**, 155111 (2007).
- [15] D. A. Abanin, E. Altman, I. Bloch, and M. Serbyn, *Rev. Mod. Phys.* **91**, 021001 (2019).
- [16] C. Monthus and T. Garel, *Phys. Rev. B* **81**, 134202 (2010).
- [17] Y. Kuno, T. Orito, and I. Ichinose, *New J. Phys.* **22**, 013032 (2020).
- [18] Y. Wang, C. Cheng, X.-J. Liu, and D. Yu, *Phys. Rev. Lett.* **126**, 080602 (2021).
- [19] D. Leykam, S. Flach, O. Bahat-Treidel, and A. S. Desyatnikov, *Phys. Rev. B* **88**, 224203 (2013).
- [20] M. Goda, S. Nishino, and H. Matsuda, *Phys. Rev. Lett.* **96**, 126401 (2006).
- [21] S. Longhi, *Opt. Lett.* **46**, 2872 (2021).
- [22] H. Li, Z. Dong, S. Longhi, Q. Liang, D. Xie, and B. Yan, *Phys. Rev. Lett.* **129**, 220403 (2022).

- [23] F. Baboux, L. Ge, T. Jacqmin, M. Biondi, E. Galopin, A. Lemaître, L. L. Gratiet, I. Sagnes, S. Schmidt, H. E. Türeci, A. Amo, and J. Bloch, *Phys. Rev. Lett.* **116**, 066402 (2016).
- [24] T. H. Harder, O. A. Egorov, J. Beierlein, P. Gagel, J. Michl, M. Emmerling, C. Schneider, U. Peschel, S. Höfling, and S. Klemmt, *Phys. Rev. B* **102**, 121302(R) (2020).
- [25] R. A. Vicencio, C. Cantillano, L. Morales-Inostroza, B. Real, C. Mejía-Cortés, S. Weimann, A. Szameit, and M. I. Molina, *Phys. Rev. Lett.* **114**, 245503 (2015).
- [26] S. Mukherjee, A. Spracklen, D. Choudhury, N. Goldman, P. Öhberg, E. Andersson, and R. R. Thomson, *Phys. Rev. Lett.* **114**, 245504 (2015).
- [27] S. Mukherjee, M. Di Liberto, P. Öhberg, R. R. Thomson, and N. Goldman, *Phys. Rev. Lett.* **121**, 075502 (2018).
- [28] S. Weimann, L. Morales-Inostroza, B. Real, C. Cantillano, A. Szameit, and R. A. Vicencio, *Opt. Lett.* **41**, 2414 (2016).
- [29] I. Bloch, J. Dalibard, and W. Zwerger, *Rev. Mod. Phys.* **80**, 885 (2008).
- [30] G.-B. Jo, J. Guzman, C. K. Thomas, P. Hosur, A. Vishwanath, and D. M. Stamper-Kurn, *Phys. Rev. Lett.* **108**, 045305 (2012).
- [31] M. Hyrkäs, V. Apaja, and M. Manninen, *Phys. Rev. A* **87**, 023614 (2013).
- [32] S. Taie, H. Ozawa, T. Ichinose, T. Nishio, S. Nakajima, and Y. Takahashi, *Sci. Adv.* **1**, e1500854 (2015).
- [33] R. Liu, W. Nie, and W. Zhang, *Sci. Bull.* **64**, 1490 (2019).
- [34] E. Giese, A. Roura, G. Tackmann, E. M. Rasel, and W. P. Schleich, *Phys. Rev. A* **88**, 053608 (2013).
- [35] F. A. An, E. J. Meier, and B. Gadway, *Phys. Rev. X* **8**, 031045 (2018).
- [36] B. Gadway, *Phys. Rev. A* **92**, 043606 (2015).
- [37] W. Gou, T. Chen, D. Xie, T. Xiao, T.-S. Deng, B. Gadway, W. Yi, and B. Yan, *Phys. Rev. Lett.* **124**, 070402 (2020).
- [38] D. Xie, T.-S. Deng, T. Xiao, W. Gou, T. Chen, W. Yi, and B. Yan, *Phys. Rev. Lett.* **124**, 050502 (2020).
- [39] H. Tasaki, *Phys. Rev. Lett.* **69**, 1608 (1992).
- [40] B. Kramer and A. MacKinnon, *Rep. Prog. Phys.* **56**, 1469 (1993).
- [41] Y.-Y. Mao, C. Zeng, Y.-R. Shi, F.-F. Wu, Y.-J. Xie, T. Yuan, W. Zhang, H.-N. Dai, Y.-A. Chen, and J.-W. Pan, companion paper, *Phys. Rev. A* **109**, 023304 (2024).
- [42] F. A. An, B. Sundar, J. Hou, X.-W. Luo, E. J. Meier, C. Zhang, K. R. A. Hazzard, and B. Gadway, *Phys. Rev. Lett.* **127**, 130401 (2021).
- [43] E. J. Meier, K. Ngan, D. Sels, and B. Gadway, *Phys. Rev. Res.* **2**, 043201 (2020).
- [44] M. Kremer, I. Petrides, E. Meyer, M. Heinrich, O. Zilberberg, and A. Szameit, *Nat. Commun.* **11**, 907 (2020).
- [45] Z.-Q. Jiao, S. Longhi, X.-W. Wang, J. Gao, W.-H. Zhou, Y. Wang, Y.-X. Fu, L. Wang, R.-J. Ren, L.-F. Qiao, and X.-M. Jin, *Phys. Rev. Lett.* **127**, 147401 (2021).